applied optics

Thick PQ:PMMA transmission holograms for free-space optical communication via wavelength-division multiplexing

Julian Gamboa,[1,4] **Tabassom Hamidfar,**[1] **Joseph Vonckx,**[2] **Mohamed Fouda,**[2] **and Selim M. Shahriar**[1,2,3,5]

[1]*Department of ECE, Northwestern University, Evanston, Illinois 60208, USA*
[2]*Digital Optics Technologies, Rolling Meadows, Illinois 60008, USA*
[3]*Department of Physics and Astronomy, Northwestern University, Evanston, Illinois 60208, USA*
[4]*e-mail: JulianGamboa2023@u.northwestern.edu*
[5]*e-mail: shahriar@northwestern.edu*

Phenantrenequinone doped poly(methyl-methacrylate) (PQ:PMMA) is a holographic substrate that can be used for angle or wavelength multiplexed Bragg gratings. However, efficient writings can be done only using a high-power, long-coherence volume laser over a limited wavelength range. This constraint makes it difficult to write gratings that would diffract several different read wavelengths into a single direction. We describe the rules for writing such gratings, taking into account the differences in the mean index seen by the write and read wavelengths. We further demonstrate the use of such a transmission hologram for wavelength-division multiplexing in a free-space optical communication system. © 2021 Optical Society of America

1. INTRODUCTION

In the late 20th century, holography was at the forefront of optical storage research due to its comparatively large theoretical storage density [1–3]. The research activities in this field, however, slowed down due to certain strong material-related limitations. One of the main issues is the balance between stability and rewritability: materials that can be rewritten, like photorefractive ferroelectric oxides (e.g., LiNbO$_3$, tend to degrade over time, while materials that are more stable, such as photorefractive polymers, can only be written once and then read repeatedly. Phenanthrenequinone (PQ)-doped poly methyl-methacrylate (PMMA) is a well-known example of the latter that has been thoroughly studied for its use in holography despite its lack of rewritability. Its ease of manufacturing, along with the long-term stability of the resulting gratings have enabled it to be used for applications other than storage, such as in the development of ultrahigh-speed correlators [4–6]. Other holographic materials like LiNbO3 have focused their development on data storage applications, although this has stagnated due to the widespread adoption of solid state memory technologies.

The two defining characteristics of holographic materials are the capacity for the absorption or refractive indices to be modified by exposure to light (writing) and the capacity to cement these modifications so that they are no longer changed with subsequent illumination (reading) [7]. By carefully controlling the "writing" light, we are able to form diffraction gratings of arbitrary shapes. Furthermore, in the case of thick holograms, these gratings always fall into the Bragg regime, diffracting efficiently only at a specific angle for a given read wavelength [8]. Because of this, it is possible to write multiple gratings at the same location but with different Bragg angles, a process known as angle multiplexing [7]. Since the Bragg angle depends on the read wavelength, it is possible to design a hologram such that different wavelengths of light will diffract at different output angles for a given common input angle, often referred to as wavelength-division demultiplexing (DeMUX). Time reversal symmetry then ensures that these different wavelengths, falling on the grating at these angles from the other side, will all emerge in the same direction. This is known as holographic wavelength-division multiplexing (HWDM) [1,9] and is useful for a variety of applications from free-space and fiber optical communication systems [10,11] to metrology.

Holographic methods present a simple technique for creating custom WDM filters and devices for various applications. While the multiplexing (MUX) capabilities are most commonly used in telecommunications, DeMUX techniques are far more widespread: some spectroscopic applications, for example, only require a few select wavelengths, and any additional diffracted light will introduce noise into the measurement [12]. This disqualifies other DeMUXing devices such as prisms, as they

generally diffract a continuous set of wavelengths. Such is the case of monocular passive ranging, wherein the intensity of three specific wavelengths is measured to estimate the distance to an emissive source [13,14]. Similarly, the snapshot method for spatial-spectral imaging benefits from the customizability of holograms [15,16], particularly if the wavelengths of interest are known beforehand.

Consider next the case of wavelength coding, which does not require any one specific wavelength but instead assigns particular data to an arbitrary channel. This is a subset of wavelength-division DeMUX'ing and benefits from the multi-channel capabilities demonstrated here. For instance, in the case of multifocal imaging the holographic device may be designed such that each wavelength focuses at a different depth and diffracts toward its own specific sensor [17]. Other authors have presented methods for achieving wavelength coding and DeMUXing for imaging and microscopy applications, demonstrating the usefulness of PQ:PMMA in many fields. Here, we derive the equations for the general case and focus on the WDM application in free-space optical communication (FSOC) systems, where the quality of the MUX and the common output trajectory are a higher priority. In particular, an ideal WDM MUX requires a wide field of view for the distinct input angles and a narrow field for the single output angle. Furthermore, cross talk is of low priority in the design process of a WDM MUX, as the input beams have different angles and wavelengths, so it is unlikely for a beam to Bragg-match more than one grating at a time in such a way that it would affect the data of another channel. In contrast, a DeMUX must prioritize the diffraction efficiency and avoid cross talk such that no information is lost or contaminated. Because the beams share a common input angle, there is a chance of diffracting from multiple gratings into the same output direction, thus contaminating the output channels. This is especially true if the wavelengths are close together, as is the case in 1550 nm FSOC systems, where the channels may only be separated by a few nanometers.

In this paper, we focus on the use of a commercially available 532 nm laser (Coherent Verdi V2) to design and write WDM holograms for three separate near infrared (NIR) wavelengths on a PQ-doped PMMA substrate. The writing wavelength was selected based on the sensitivity of the PQ dye and the availability of lasers with high intensity and large coherence volume. We present the experimental results demonstrating WDM FSOC with this system as a proof of principle. This technique will be extended in the near future to realize free-space optical communication with lasers around the eye-safe wavelength of 1550 nm using a much larger number of channels.

2. ANGLE MULTIPLEXING ON THICK HOLOGRAPHIC SUBSTRATES

Holograms are formed when two laser beams of the same wavelength and polarization generate an interference pattern in a photosensitive medium, such as a PQ:PMMA substrate. A modulation of the refractive index is created due to the different reactions of the substrate to the peaks and troughs of the pattern [18]. Like any other Bragg grating, efficient first-order diffraction only occurs when the Bragg condition is met. This property

can be exploited to create multiple spatially overlapping holograms that will not interfere with one another for proper choice of operating parameters. PQ:PMMA, however, is only sensitive to a small range of wavelengths, severely limiting the possibility of varying the write wavelength. We can circumvent this issue altogether by designing a single-wavelength writing system that can create holograms with arbitrary orientations and periodicities, such that the Bragg condition is met at any desired set of wavelengths and angles.

What follows is a brief mathematical derivation of the equations that link the write wavelength (λ_w) and angles (θ_1, θ_2) to the read wavelength (λ_R) and angles (α_1, α_2) for a single grating. To begin, we assume that the beams will initially be traveling in air and so the angles must change when they come in contact with the PQ:PMMA substrate. We will denote the refracted angles as $\alpha'_{1,2}$ and $\theta'_{1,2}$ for the read and write beams, respectively. Using Snell's law, these are

$$\alpha'_{1,2} = \sin^{-1}\left(\frac{1}{n_R}\sin\left(\alpha_{1,2}\right)\right)$$

$$\theta'_{1,2} = \sin^{-1}\left(\frac{1}{n_w}\sin\left(\theta_{1,2}\right)\right), \tag{1}$$

where n_R and n_w denote the average refractive index of PMMA at the read and write wavelengths, respectively. When the writing beams interfere, the periodicity of the resulting grating will be dependent on the difference of the writing K-vectors ($\vec{K}_{W1}$, $\vec{K}_{W2}$) [19]:

$$\vec{K}_W = \vec{K}_{W1} - \vec{K}_{W2}$$

$$= \frac{2\pi n_w}{\lambda_w}\left(-\sin\left(\theta'_1\right) - \sin\left(\theta'_2\right)\right)\hat{i}_x$$

$$+ \frac{2\pi n_w}{\lambda_w}\left(\cos\left(\theta'_1\right) - \cos\left(\theta'_2\right)\right)\hat{i}_z. \tag{2}$$

Here, we have defined the light to be propagating in the *x-z* plane as shown in Fig. 1(a).

Obviously, different combination of wavelength and angles can generate the same grating; as can be seen here, for a longer wavelength (shorter wavenumber) the angles have to be larger. We now analyze the Bragg-matching condition to find the angles in question. First, consider that the grating will have a fixed periodicity

$$\vec{K}_R = \vec{K}_W \equiv \vec{K}, \tag{3}$$

where

$$\vec{K}_R = \frac{2\pi n_R}{\lambda_R}\left(-\sin\left(\alpha'_1\right) - \sin\left(\alpha'_2\right)\right)\hat{i}_x$$

$$+ \frac{2\pi n_R}{\lambda_R}\left(\cos\left(\alpha'_1\right) - \cos\left(\alpha'_2\right)\right)\hat{i}_z. \tag{4}$$

Combining Eqs. (2)–(4), we find that

$$\sin\left(\theta'_2\right) + \sin\left(\theta'_1\right) = \frac{\lambda_w\, n_R}{\lambda_R\, n_w}\left(\sin\left(\alpha'_2\right) + \sin\left(\alpha'_1\right)\right),$$

$$\cos\left(\theta'_2\right) - \cos\left(\theta'_1\right) = \frac{\lambda_w\, n_R}{\lambda_R\, n_w}\left(\cos\left(\alpha'_2\right) - \cos\left(\alpha'_1\right)\right). \tag{5}$$
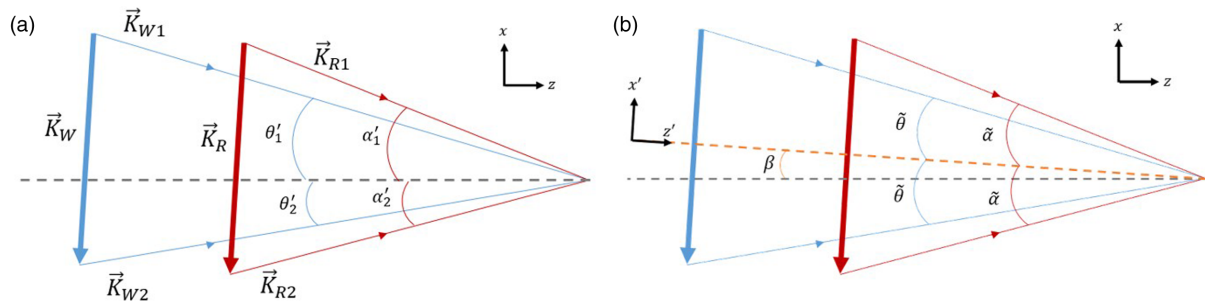
Fig. 1. K-vector diagram of the write and read beam angles within the substrate. Note that $\vec{K}_W$ and $\vec{K}_R$ are identical. The y and y' axes are facing into the paper (a) original (x, y, z) coordinate system. This is defined by the substrate itself such that the front face of the substrate is in the x-y plane and the bottom is in the y-z plane. (b) Rotated coordinate system (x', y', z'), which is defined such that the incoming beams are symmetric around the z' axis as shown in Fig. 1(b). The θ'_1 angle is defined by $\theta'_1 = \tan^{-1}(|\vec{K}_{W1} \cdot \hat{x}|/|\vec{K}_{W1} \cdot \hat{z}|)$. All other angles are defined in the same way with their respective K-vectors in their corresponding coordinate system, such that they are always positive with a value between 0° and 90°.

To solve these equations, we rotate our coordinate system by an angle β such that $\vec{K}$ is parallel to the x' axis and the incoming beams are symmetric around the z' axis as shown in Fig. 1(b). We can relate the relevant angles in the original and rotated coordinate systems as follows:

$$\tilde{\alpha} = \frac{\alpha'_1 + \alpha'_2}{2} \quad \tilde{\theta} = \frac{\theta'_1 + \theta'_2}{2}$$

$$\alpha'_1 = \tilde{\alpha} + \beta \quad \theta'_1 = \tilde{\theta} + \beta$$

$$\alpha'_2 = \tilde{\alpha} - \beta \quad \theta'_2 = \tilde{\theta} - \beta. \tag{6}$$

Combining these equations, we find the rotation angle to be

$$\beta = \alpha'_1 - \tilde{\alpha} = \frac{\alpha'_1 - \alpha'_2}{2}. \tag{7}$$

We can now rewrite the K-vectors in the new rotated coordinate system trivially:

$$\vec{K}_R = -\frac{4\pi n_R}{\lambda_R} \sin(\tilde{\alpha}) \, \hat{i}_{x'},$$

$$\vec{K}_W = -\frac{4\pi n_w}{\lambda_w} \sin(\tilde{\theta}) \, \hat{i}_{x'}. \tag{8}$$

Combining this with Eqs. (3), (6), and (7), we find

$$\tilde{\theta} = \sin^{-1}\left(\frac{\lambda_w \, n_R}{\lambda_R \, n_w} \sin(\tilde{\alpha})\right), \tag{9}$$

which, after substituting $\tilde{\alpha}$ and $\tilde{\theta}$, yields

$$\theta'_1 = \sin^{-1}\left(\frac{\lambda_w \, n_R}{\lambda_R \, n_w} \sin\left(\frac{\alpha'_1 + \alpha'_2}{2}\right)\right) + \frac{\alpha'_1 - \alpha'_2}{2}, \tag{10}$$

$$\theta'_2 = \sin^{-1}\left(\frac{\lambda_w \, n_R}{\lambda_R \, n_w} \sin\left(\frac{\alpha'_1 + \alpha'_2}{2}\right)\right) - \frac{\alpha'_1 - \alpha'_2}{2}. \tag{11}$$

Finally, we may use Snell's law to find the equivalent angles for the beams in air as was done in Eq. (1). With these equations, we can determine the necessary write angles $(\theta_{1,2})$ for a given writing wavelength (λ_w) and refractive index in PMMA (n_w) for

a given set of the corresponding reading parameters $(\alpha_{1,2}, \lambda_R,$ and $n_R)$.

There are many ways to control the input angle of the two beams. For our demonstration, we used the setup shown in Fig. 2(a). Here, M1, M2, and the hologram are placed on motorized rotation stages. The position of the hologram directly determines θ_2, while a combination of the positions of the three moving components determines θ_1. Figure 2(b) shows the geometry of the equilateral triangle setup used for the writing process. The angles of rotation of M1 and M2 are denoted α and β, respectively. The mirrors are placed such that, when they are in their initial position ($\alpha = \beta = 0°$, shown in green), they are parallel to the vertical axis, and the beam will always reflect off of the rotation vertex. The hologram is then located in line with M1 at the intercept with the reflected beam. In this way, we find that the distance between the M1 vertex, and the point of contact between the beam and the hologram will be given by $y_1 + y_2 = 2x/\tan(\theta_i)$, where x is the horizontal distance between M2 and both M1 and the hologram. When the mirrors are rotated ($\alpha \neq 0°$, $\beta \neq 0°$ shown in red), the new vertical distance between the two points and the new horizontal distance with M2 will be

$$y'_1 + y'_2 = \frac{x'}{\tan(\theta_i - 2\alpha)} + \frac{x'}{\tan(\theta_i - 2\alpha + 2\beta)}$$

$$x' = x\left(1 - \frac{\sin(2\alpha)\sin(\beta)}{\sin(\theta_i)\sin(\theta_i + \beta - 2\alpha)}\right). \tag{12}$$

Interestingly, when $\beta = 2\alpha$ and the mirror vertices form an equilateral triangle ($\theta_i = 60°$), the vertical distance becomes

$$y'_1 + y'_2 = x\left(1 - \frac{\sin^2(2\alpha)}{\sin^2(\theta_i)}\right)\left(\frac{1}{\tan(\theta_i - 2\alpha)} + \frac{1}{\tan(\theta_i + 2\alpha)}\right)$$

$$= \frac{2x}{\tan(\theta_i)}, \tag{13}$$

which is the same as the value when $\alpha = \beta = 0°$. Thus, by rotating mirror M2 by twice the rotation of mirror M1, the beam will always intersect the hologram at the same position, albeit at a distinct angle. The resulting intercept angle with respect to the vertical axis will be given by $\phi_{\text{Holo}} = \theta_i + 2\alpha = 60° + 2\alpha$.
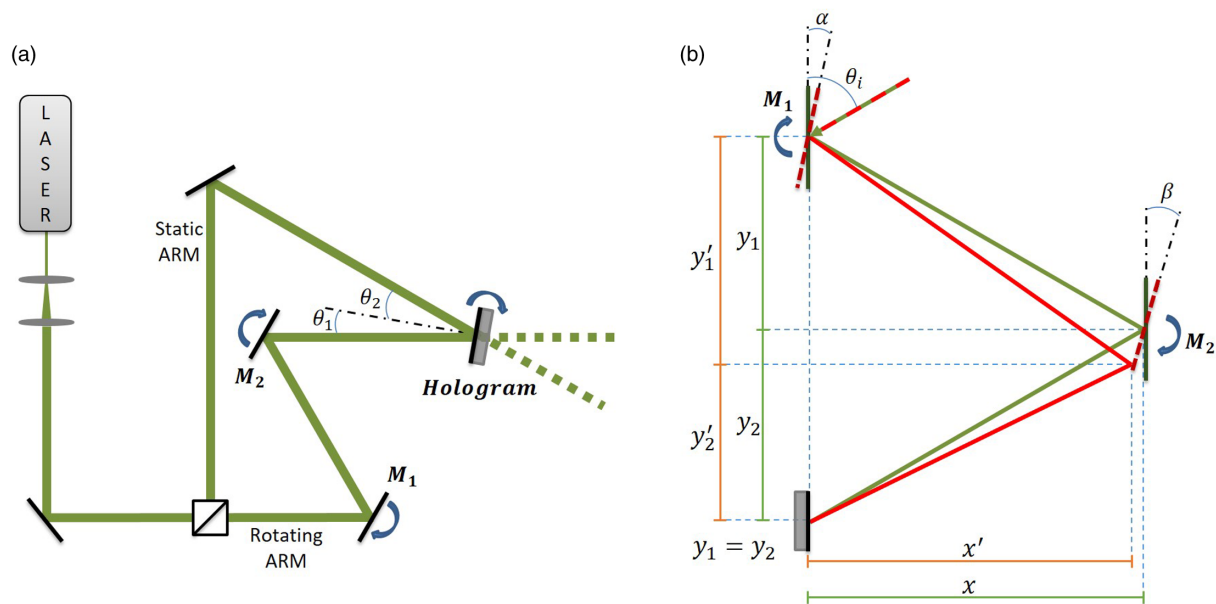
Fig. 2. (a) Angle multiplexing writing setup. Mirror M1, mirror M2, and the hologram are placed on motorized rotation stages. The position of the hologram determines the angle θ_2, while a combination of the positions of the three moving components determines θ_1. The angles are measured with respect to the normal of the substrate. (b) Geometry of the equilateral triangular setup used in (a) when mirrors M1 and M2 are rotated by angles α and β, respectively (red), and when the mirrors are at their starting position $\alpha = \beta = 0°$ (green). The original beam (green and red dashes) is unchanging and always makes an angle θ_i with the vertical axis. All rotation angles are measured relative to the vertical axis in the clockwise direction.

For our experiments, a 532 nm Coherent Verdi V2 laser provided the writing beam, which was expanded to a diameter of 25.4 mm prior to being separated into the two writing arms. A refractive index of $n_w = 1.494$ was considered for the writing beam. All refractive indices were obtained from reference [20]. A 532 nm writing beam was chosen due to the material photosensitivity and the availability of stable commercial lasers with high power and narrow linewidth at this wavelength.

3. RESULTS OF A 3× MULTIPLEXER FOR 760, 780, AND 795 nm

To test the WDM characteristics of PMMA, we relied on the three-mirror system described in the previous section, using substrates that ranged in thickness between 1.3 and 2.8 mm. The gratings were to be written for 760, 780, and 795 nm. The material thickness relates nontrivially to the diffraction efficiency [19] and wavelength [21], and as such special care must be taken when constructing the substrate. When MUXing holograms at these wavelengths, the refractive index modulation for each grating typically falls in the regime where the diffraction efficiency monotonically increases over the selected thickness range. However, as the thickness is incremented, this causes increased absorption during the writing process, as well as a higher probability of bubbling and distortions during fabrication, which leads to a point of diminishing returns.

Using Eqs. (10) and (11) derived in the previous section, and considering that for WDM we desire one of the output angles to be equal for all wavelengths, we obtained the corresponding write angles at 532 nm and programmed our motorized rotation stages to achieve them. Various exposure schedules were written
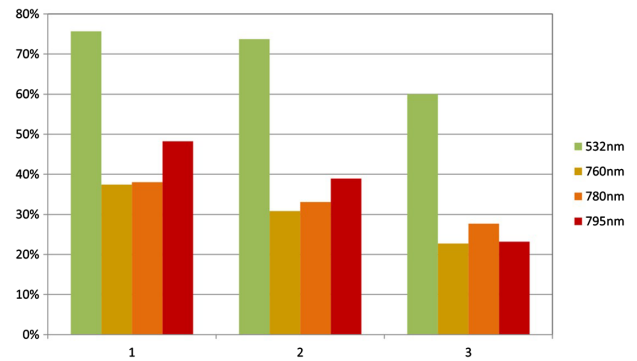
Fig. 3. Diffraction efficiency of three multiplexed holograms (1, 2, and 3) at wavelengths of 532, 760, 780, and 795 nm.

at different locations on each sample. Figure 3 shows the diffraction efficiencies of all three multiplexed holograms at a single location for four separate wavelengths. The diffraction efficiency is obtained by measuring the transmitted and diffracted power at each wavelength and using the following formula: $\eta_{\mathrm{diff}} = P_d/(P_t + P_d)$, where P_d is the diffracted power, P_t is the transmitted power, and η_{diff} is the efficiency. This sample had a thickness of 2.5 mm and a base exposure of $40.4\,\mathrm{J} * \mathrm{cm}^{-2}$, increasing by a factor of 1.26 between each hologram. It is clear that the maximum diffraction efficiency was achieved for the writing wavelength (532 nm). We also note that the first hologram achieved the highest efficiency, dropping by a value of between 10%–15% by the third hologram for all wavelengths. It may be possible to improve this by modifying the exposure schedule to have a more energetic exposure for the last hologram [22,23].
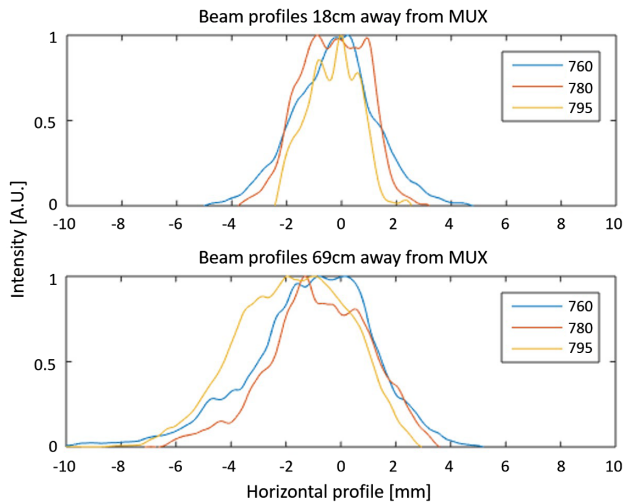
Fig. 4. Horizontal beam profiles for 760, 780, and 795 nm beams input at their corresponding angles and output at a multiplexed angle: (a) 18 cm away from the multiplexer and (b) 69 cm away from the MUX.

Figure 4 shows the horizontal profiles of three simultaneously diffracted beams at our desired wavelengths, where the input angles correspond to those calculated above. The profiles were measured by placing a camera at a fixed point a distance away from the hologram on the shared output path and capturing one profile at a time. It is evident that, despite expanding, the three beams maintain essentially the same path. Because each beam was input at its own separate angle, sharing a common output angle for their respective holograms, they have been multiplexed. The angular full width at half-maximum (FWHM) was measured to be less than 0.1° for each hologram at 532 nm, which was the resolution limit of our instruments. The angular selectivity of one of the holograms in this disk is shown for the relevant wavelengths in Fig. 5.
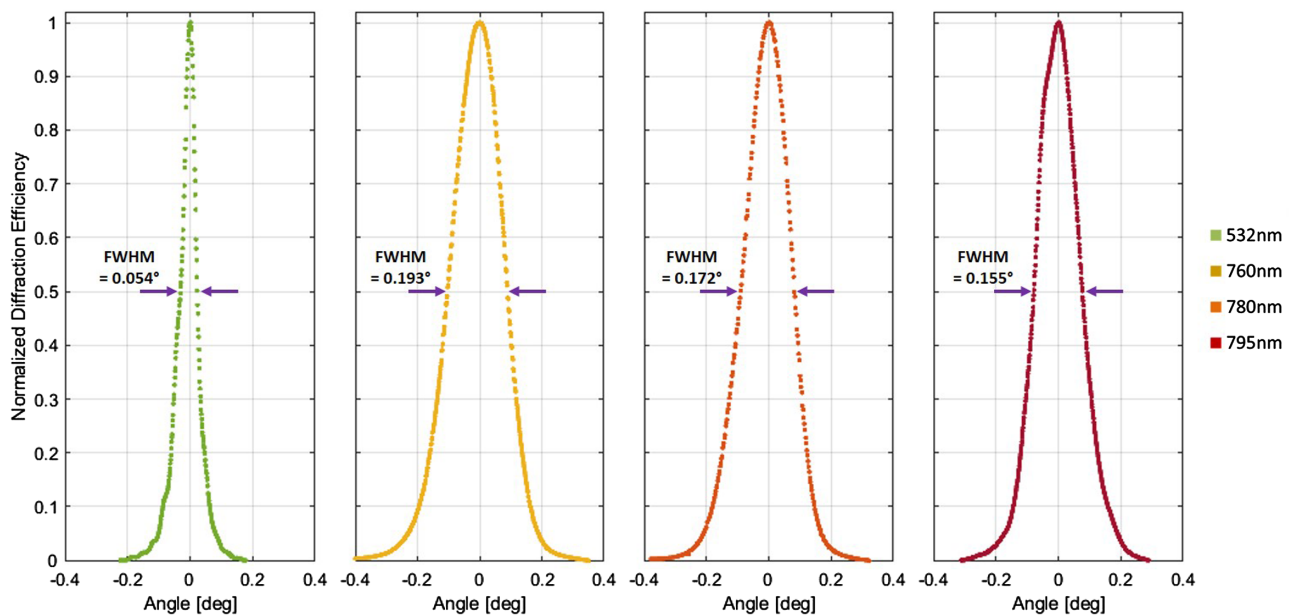
According to Kogelnik's coupled wave theory [19,24] for unslanted transmission gratings, the amplitude of the index modulation Δn is related to the diffraction efficiency η_{diff} as follows:

$$\Delta n = \frac{\lambda \cos(\theta)}{\pi d} \sin^{-1}\left(\sqrt{\eta_{\text{diff}}}\right), \tag{14}$$

where d is the thickness, λ is the read wavelength, and θ is the input angle. Using this formula in combination with our experimental data, we estimated the maximum refractive index modulation to be $\Delta n_1 = 6.880 \times 10^{-5}$, $\Delta n_2 = 6.704 \times 10^{-5}$, and $\Delta n_3 = 5.713 \times 10^{-5}$ for the first, second, and third holograms, respectively. The differences in the values of the index modulation at different wavelengths can in general be attributed to the relative detuning of these frequencies away from the effective two-level resonance frequency of the PQ:PMMA system. A detailed investigation of this dependence, as well as a systematic investigation for optimizing the diffraction efficiency at wavelengths of practical interest in free-space optical communication, will be presented in another paper under preparation [21]. In separate samples we have achieved index modulations on the order of 5×10^{-4}, which agrees with what has been reported by other authors [10].

A thick holographic grating has two possible input angles where the Bragg condition is met; whichever we do not use for the input will automatically be the output angle. Because of this, if we have a multiplexed output and use it as an input for a separate disk of the same design but select the new input angle to be equal to the first disk's output angle, the second disk will function as a demultiplexer (DeMUX). To test this, we constructed a simple 3× WDM channel using one hologram to multiplex three beams and another to DeMUX them; Fig. 6 shows a simplified diagram of the setup. We then amplitude modulated the input beams independently through motorized shutters and recorded the output of the DeMUX hologram.

Fig. 5. Angular selectivity curves for 532, 760, 780, and 795 nm. The smallest FWHM was measured to be 0.054° for the writing beam at 532 nm. The FWHM for the multiplexing wavelengths has an average value of 0.173°.
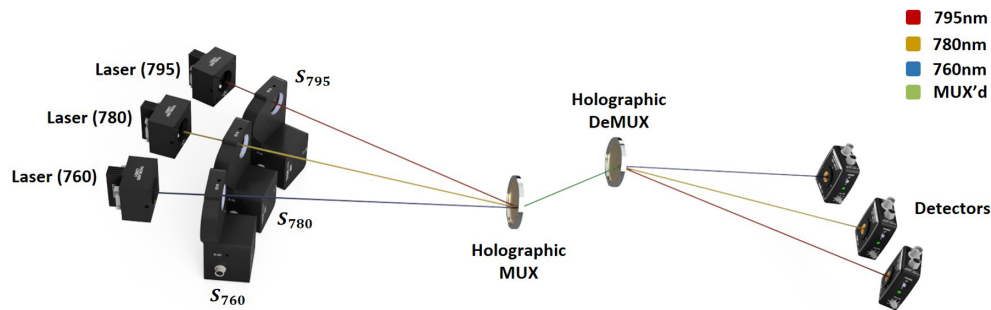
Fig. 6. Simple 3× WDM channel constructed using two holographic MUX/DeMUX disks. Each laser was fitted with a motorized shutter (labelled "S") in order to use binary amplitude modulation for each independent channel.
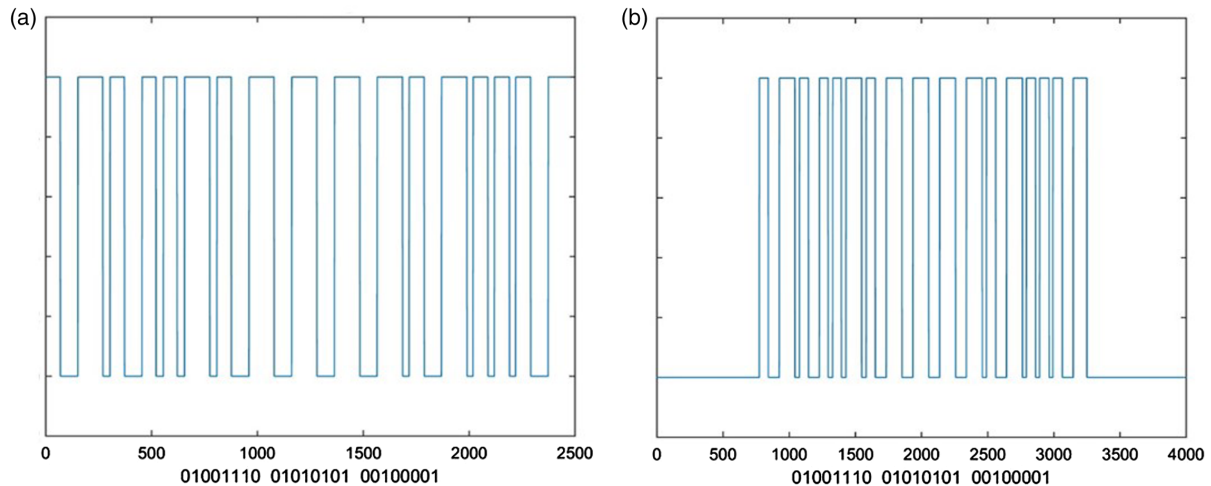
Fig. 7. 3× WDM results for only the 795 nm channel. The horizontal axis shows time in units of milliseconds. (a) Transmitted bitstream with Manchester encoding, corresponding to the three-character string "NU!" in ASCII. (b) Signal measured after the DeMUX hologram, quantized to remove noise (threshold was set at half of the maximum measured value). No errors were detected in the bitstream.

The use of mechanical shutters meant that the amplitude modulation would be binary, i.e., blocking or unblocking the laser in its entirety.

The transmitted data was successfully received in parallel. Figure 7 shows a sample of the transmitted and received data. The information was prepared with Manchester encoding and transmitted by blocking and unblocking each individual laser, thus achieving binary amplitude modulation. This encoding scheme allows for clockless transmission of data, where a "0" is represented by a falling edge symbol (i.e., one that starts "high" and ends "low"), and a "1" is represented by a rising edge symbol (i.e., one that starts "low" and ends "high"). The data is thus received asynchronously and subsequently quantized with a threshold placed at the mean intensity. Figure 7(a) shows the computer-generated bitstream prior to transmission. In Fig. 7(b), the leading and trailing values with zero intensity indicate that there was no information received during that time. This method for transmission is inefficient, as each symbol only corresponds to one bit, but its simplicity allows us to evaluate the holographic MUX/DeMUX independently of other factors. We observe that the transmitted and received data present a perfect match, proving that the holographic MUX/DeMUX is functioning as expected.

4. SUMMARY AND DISCUSSION

Multiple holographic gratings were written to the same spot on a PQ:PMMA substrate, such that they all shared the same output angle for distinct input angles when using specific wavelengths. The beams clearly diffracted without cross talk at an angular FWHM of less than 0.1° per channel as measured at 532 nm, demonstrating the feasibility of this mechanism for WDM in FSOC systems. For a practical FSOC system, it would be necessary to employ lasers at a range of wavelengths that are eye safe. Lasers operating at wavelengths around 1550 nm would satisfy this requirement. Work is currently underway for optimizing the diffraction efficiency of gratings in this band [17]; this would be followed by a demonstration of a holographic WDM-based FSOC system in this band.

While mature WDM systems exist for optical communication, these are generally constructed in a manner that is well suited for coupling to optical fibers. In principle, one could combine these with an array of mirrors and lenses to realize WDM systems for FSOC. However, the holographic WDM we have demonstrated here obviates the need for any such additional optical components, which are generally bulky and ill-suited for typical platforms (such as unmanned aerial vehicles).

The WDM system we have demonstrated here is meant as a proof of principle for the efficacy of such a system. As such, we have used lasers at wavelengths that are not suitable for a practical FSOC system. However, it should be noted that a holographic WDM employing these wavelengths can also be of practical utility for some spectroscopic applications, such as laser ranging employing differential atmospheric absorption [18]. In such a system, a broadband light would pass through the atmosphere and then enter the hologram at a particular DeMUX angle, diffracting the desired wavelengths in predetermined directions where they can be measured in parallel. Known atmospheric absorption coefficients at the three wavelengths employed here can then be used to infer the distance of the source.

Disclosures. The authors declare no conflict of interest.

Data Availability. Data underlying the results presented in this paper are not publicly available at this time but may be obtained from the authors upon reasonable request.

REFERENCES

1. H.-Y. S. Li and D. Psaltis, "Three-dimensional holographic disks," Appl. Opt. **33**, 3764–3774 (1994).
2. A. Adibi, K. Buse, and D. Psaltis, "Multiplexing holograms in LiNbO₃: Fe: Mn crystals," Opt. Lett. **24**, 652–654 (1999).
3. S. H. Lin, K. Y. Hsu, W. Chen, and W. T. Whang, "Phenanthrenequinone-doped poly (methyl methacrylate) photopolymer bulk for volume holographic data storage," Opt. Lett. **25**, 451–453 (2000).
4. J. Gamboa, M. Fouda, and S. M. Shahriar, "Demonstration of the hybrid opto-electronic correlator for shift, scale, and rotation invariant target recognition," Opt. Express **27**, 16507–16520 (2019).
5. D. Casasent and D. Psaltis, "Position, rotation, and scale invariant optical correlation," Appl. Opt. **15**, 1795–1799 (1976).
6. J. Gamboa, T. Hamidfar, and S. M. Shahriar, "Integration of a PQ:PMMA holographic memory device into the hybrid optoelectronic correlator for shift invariant target recognition," submitted to Optics Express.
7. K. Curtis, L. Dhar, and P. A. Blanche, "Holographic data storage technology," Opt. Digit. Image Process. Fundam. Appl. **44**, 227–250 (2011).
8. A. Heifetz, J. T. Shen, S. C. Tseng, G. S. Pati, J. K. Lee, and M. S. Shahriar, "Angular directivity of diffracted wave in Bragg-mismatched readout of volume holographic gratings," Opt. Commun. **280**, 311–316 (2007).
9. J. Qiao, F. Zhao, J. Liu, and R. T. Chen, "Dispersion-enhanced volume hologram for dense wavelength-division demultiplexer," IEEE Photon. Technol. Lett. **12**, 1070–1072 (2000).
10. A. Sato and R. K. Kostuk, "Holographic grating for dense wavelength division optical filters at 1550 nm using phenanthrenquinone-doped poly(methyl methacrylate)," Proc. SPIE **5216**, 44–52 (2003).
11. S. Shimizu, A. Okamoto, F. Mizukawa, K. Ogawa, A. Tomita, T. Takahata, S. Shinada, and N. Wada, "Volume holographic spatial mode demultiplexer with a dual-wavelength method," Appl. Opt. **57**, 146–153 (2018).
12. M. R. Hawks, R. A. Vincent, J. Martin, and P. Perram, "Short-range demonstrations of monocular passive ranging using O₂ (X3Σg⁻ → b1Σg⁺) absorption spectra," Appl. Spectrosc. **67**, 513–519 (2013).
13. H. Yu, B. Liu, Z. Yan, and Y. Zhang, "Passive ranging using a filter-based non-imaging method based on oxygen absorption," Appl. Opt. **56**, 7803–7807 (2017).
14. J. Gamboa, J. Vonckx, M. Fouda, and S. M. Shahriar, "PQ:PMMA holographic wavelength division multiplexing filters for use in monocular passive ranging and free space optical communications," in Frontiers in Optics/Laser Science (2020).
15. Q. Li, X. He, Y. Wang, H. Liu, D. Xu, and F. Guo, "Review of spectral imaging technology in biomedical engineering: achievements and challenges," J. Biomed. Opt. **18**, 100901 (2013).
16. S. Vyas, Y.-H. Chia, and Y. Luo, "Volume holographic spatial-spectral imaging systems [Invited]," J. Opt. Soc. Am. A **36**, A47–A58 (2019).
17. Y. Luo, S. B. Oh, and G. Barbastathis, "Wavelength-coded multifocal microscopy," Opt. Lett. **35**, 781–783 (2010).
18. Y. Hsiao, W.-T. Whang, and S. H. Lin, "Analyses on physical mechanism of holographic recording in phenanthrenequinone-doped poly(methyl methacrylate) hybrid materials," Opt. Digit. Image Process. Fundam. Appl. **43**, 1993–2002 (2004).
19. H. Kogelnik, "Coupled wave theory for thick hologram gratings," Bell Syst. Tech. J. **48**, 2909–2947 (1969).
20. G. Beadie, M. Brindza, R. A. Flynn, A. Rosenberg, and J. S. Shirk, "Refractive index measurements of poly(methyl methacrylate) (PMMA) from 0.4–1.6 μm," Appl. Opt. **54**, F139–F143 (2015).
21. J. Gamboa, T. Hamidfar, J. Bonacum, and S. M. Shahriar, "Determination of the refractive index modulation of PQ:PMMA holographic phase gratings over a large spectral range through a two-level approximation of the electric susceptibility," submitted Optical Materials Express.
22. A. Pu, K. Curtis, and D. Psaltis, "Exposure schedule for multiplexing holograms in photopolymer films," Opt. Eng. **35**, 2824–2829 (1996).
23. S. Lin, K. Y. Hsu, W. Chen, and W. Whang, "Exposure schedule for multiplexing holograms in photopolymer," Proc. SPIE **3801**, 100–106 (1999).
24. O. Beyer, I. Nee, F. Havermeyer, and K. Buse, "Holographic recording of Bragg gratings for wavelength division multiplexing in doped and partially polymerized poly(methyl methacrylate)," Appl. Opt. **42**, 30–37 (2003).